

Catalyst-Free Metalorganic Chemical-Vapor Deposition of Ultrafine ZnO Nanorods

Won Il PARK, Jinkyong YOO and Gyu-Chul YI*

National CRI Center for Semiconductor Nanorods and Department of Materials Science and Engineering, Pohang University of Science and Technology, Pohang 790-784

(Received 7 March 2005, in final form 15 March 2005)

We report on the catalyst-free growth and the photoluminescent (PL) properties of ultrafine ZnO nanorods. Employing metalorganic chemical-vapor deposition, we prepared ultrafine ZnO nanorods, with very thin diameters below 10 nm, on Si substrates at growth temperatures of 800 – 1000 °C without using any metal catalyst. Synchrotron radiation X-ray diffraction and transmission electron microscopy measurements revealed that those nanorods were single crystalline. Furthermore, from the PL spectra of the ultrafine ZnO nanorods, a systematic blue-shift in their PL peak position was observed with decreasing diameter, presumably due to the quantum-confinement effect along the radial direction in ZnO nanorods.

PACS numbers: 61.46.+w, 68.65.-k, 78.67.-n, 81.07.-b

Keywords: ZnO nanorod, Catalyst-free MOCVD, Ultrafine nanorod, Quantum confinement

I. INTRODUCTION

One-dimensional (1D) semiconductor nanostructures have attracted a lot of attention for their unique applications in mesoscopic physics [1, 2] and the possibility that they may be used as building blocks of biological and chemical molecule nanosensors [3] as well as electronic [4–6] and photonic [7–9] nanodevices. Intensive research has focused on fabricating 1D semiconductor nanostructures and investigating the quantum-size effect and the dependence of the electrical transport or optical properties on dimensionality [10–12]. Although narrow-bandgap semiconductor nanowires have easily exhibited quantum-confinement effects along a radial direction [11], the quantum effects for wide bandgap semiconductor nanomaterials, such as ZnO, GaN, ZnSe, and ZnS, have rarely been reported. Since the wide-bandgap materials exhibit an exciton Bohr radius (a_B) in the range of $\sim 2 - 4$ nm [13], the quantum effect in the 1D nanomaterials can be significantly observed only if their diameter is smaller than several nanometers [14, 15]. However, it has been very difficult to prepare oxide semiconductor nanowires and nanorods with diameters thinner than 10 nm. Only a few works have addressed the synthesis of ultrafine nanowires (nanorods) below 10 nm and the observation of a weak carrier-confinement effect in the radial direction [16, 17]. Furthermore, diameter-controllable preparation of ultrafine ZnO nanowires and nanorods has not been reported. In this paper, we report the reproducible preparation of ultrafine ZnO nanorods by using

a simple change of growth temperature in catalyst-free metalorganic chemical-vapor deposition (MOCVD).

Catalyst-free MOCVD of semiconductor nanorods has unique advantages over catalyst-assisted methods because this method offers vertically aligned growth of high-purity single crystalline nanorods with uniform diameter and length distributions [18]. Nevertheless, controls of the nanorod dimension and the aspect ratio, as well as the density and the growth sites, have been very difficult. The nanorod diameter and the aspect ratio in the catalyst-free MOCVD depend on the growth temperature, the reactant gas flow rate, and the growth time. In this research, we showed that the growth temperature was one of the most important parameters in determining the diameter and the aspect ratio of nanorods. Furthermore, the ultrafine ZnO nanorods exhibited a blueshift of the excitonic PL emission peaks, strong evidence of the quantum-confinement effect.

II. EXPERIMENT

Ultrafine ZnO nanorods were grown on Si substrates by using catalyst-free MOCVD. Although the reactant gas flow rates, the growth time, and the growth temperature in this method affect the diameter and the aspect ratio of the ZnO nanorods, we could control the nanorod size simply by changing the growth temperature. Prior to ZnO nanorod growth, 10-nm-thick ZnO buffer layers were initially deposited at room temperature, and the substrate temperature was slowly increased to a nanorod growth temperature of 800 – 1000 °C with a ramp rate

*E-mail: gcyi@postech.ac.kr; Fax: +82-54-279-8635

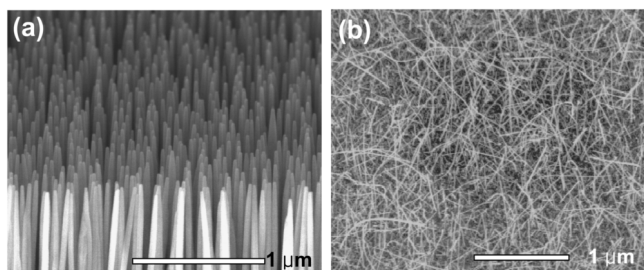


Fig. 1. FE-SEM images of (a) thick ZnO nanorods with a mean diameter of 35 nm and (b) ultrafine ZnO nanorods with a mean diameter of 9 nm.

of 50 °C/min. During nanorod growth, the flow rates of oxygen and DEZn flow, which were used as the reactants, were in the range of 20 sccm and 1.0 – 3.0 sccm at a DEZn bubbler temperatures of – 15 °C, respectively. Typical growth times were in the range of 0.5 – 2 hour. Thick ZnO nanorods with diameters above 20 nm were also grown at a low temperature of 400 – 600 °C, as previously reported elsewhere [18].

The structural and the optical characteristics of the ultrafine ZnO nanorods were investigated using synchrotron radiation X-ray diffraction (SR-XRD), scanning electron microscopy (SEM), transmission electron microscopy (TEM), and PL spectroscopy. The SR-XRD measurements of ZnO nanorods were performed in the 8C2 high-resolution powder diffraction beamline at the Pohang Accelerator Laboratory. A field-emission TEM (Philips 300 kV) with a 1.7-Å point resolution was used for structural characterizations of ultrafine ZnO nanorods. The PL spectra of the ZnO nanorods were measured at room temperature by using the 325-nm line of a He-Cd laser as an excitation source. The details of the TEM and the PL measurements are described elsewhere [18].

III. RESULTS AND DISCUSSION

The size and the morphology of ZnO nanorods grown by using catalyst-free MOCVD strongly depend on the growth temperature, the growth time, and the reactant gas flow rates. We grew ZnO nanorods at different growth temperatures in order to investigate changes in the size and morphology of ZnO nanorods with growth temperature. Figures 1(a) and (b) show the field-emission SEM (FE-SEM) images of ZnO nanorods grown at 500 and 800 °C for 1 hr, respectively. The ultrafine ZnO nanorods grown at 800 °C exhibited a very thin diameter of 9 nm and a long length of above 3-μm while the ZnO nanorods grown at 500 °C showed a mean diameter of 30 – 45 nm. In general, the mean diameter of ZnO nanorods decreased with increasing temperature, and ultrafine ZnO nanorods were grown at 700 – 1000 °C while vertically well-aligned thick ZnO nanorods were grown at 400 – 600 °C.

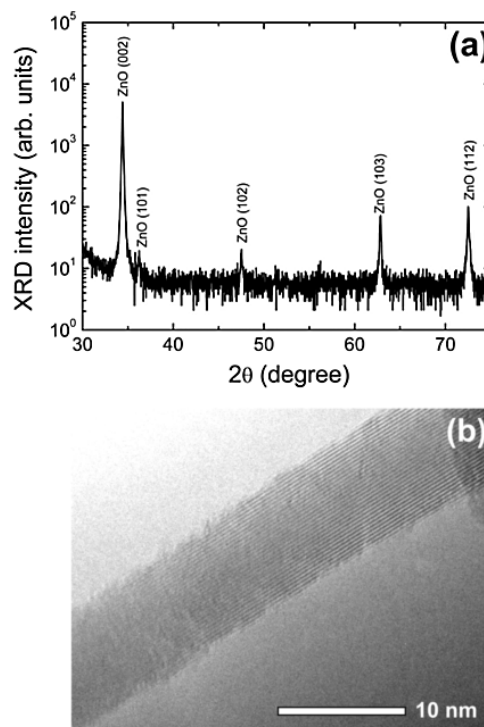


Fig. 2. (a) SR-XRD patterns of ultrafine ZnO nanorods. (b) HR-TEM images of ultrafine ZnO nanorods with a mean diameter of 8 nm.

Kinetics depending on the growth condition and surface-energy minimization during the crystallization might be responsible for the formation of thinner ZnO nanorods with a higher aspect ratio at higher growth temperature, but the exact nanorod growth mechanisms are not yet clear. From the *ab-initio* total-energy calculations [19], the surface energy of the (0001)-Zn and (000 $\bar{1}$)-O planes (4.00 J/m²) as polar facets is larger than that of nonpolar planes, such as the (01 $\bar{1}$ 0) and the (2 $\bar{1}$ $\bar{1}$ 0) facets (2.32 J/m²). Due to the surface energy of the hexagonal (0001) plane of ZnO being highest, stacking along the [0001] direction was energetically favorable [20]. As the growth temperature was increased, atomic desorption from (01 $\bar{1}$ 0) planes with a relatively low surface energy, migration to stable positions, and adsorption to the (0001) planes with the highest surface energy may be enhanced. Accordingly, ultrafine ZnO nanorods with higher aspect ratios were obtained at an elevated growth temperature.

Figure 2(a) shows SR-XRD θ - 2θ scan results of ultrafine ZnO nanorods. The SR-XRD θ - 2θ scan data taken from the ultrafine ZnO nanorods demonstrated that they had a wurtzite structure with *c*-axis lattice parameter of \sim 5.2 Å, which is quite similar to the reported value of bulk ZnO (5.207 Å) [21]. The observation of only ZnO-related XRD peaks within the detection limit of SR-XRD and the strong diffraction intensity relative to the background signal indicate that the ZnO nanorods are highly crystalline.

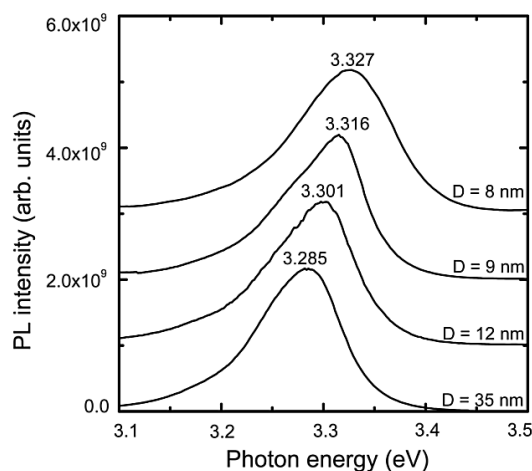


Fig. 3. Room temperature PL spectra of both ultrafine and thick ZnO nanorods with different mean diameters of 8 ± 3 nm, 9 ± 3 nm, 12 ± 3 nm, and 35 ± 4 nm.

More detail on the crystal structure of ultrafine ZnO nanorods was obtained by using high-resolution TEM (HR-TEM). The HR-TEM image in Fig. 2(b) shows that the diameter of an ultrafine ZnO nanorod is as small as 7 nm with a normalized standard deviation value (standard deviation divided by the mean) of 0.2 – 0.3. Furthermore, the TEM images displayed a highly ordered lattice image of the ultrafine ZnO nanorod, indicating that the ZnO nanorods were almost defect-free and single crystalline.

The observation of defect-free high crystallinity in ultrafine ZnO nanorods grown by using catalyst-free MOCVD is different from a previous work that reported observation of distortion and dislocations in ZnO nanobelts based on the vapor-liquid-solid (VLS) process [17]. According to Wang's explanation, ZnO nanobelts are mainly synthesized via a root-growth process; *i.e.*, growth of nanobelts occurred via precipitation on the ZnO/metal alloy droplets remaining on the substrate. In this case, a large local strain originating from nanobelt bending introduced distortion in the orientation of the (0001) atomic planes and led to the formation of edge dislocations, and thereby resulting in the formation of curly shaped nanobelts. However, in catalyst-free MOCVD, ZnO nanorods are grown along the *c*-axis by direct adsorption of gas phase molecules mainly on the nanorod tips. Hence, in this process, the bending-induced strain is reduced, minimizing the formation of edge dislocations or stacking faults in ultrafine nanorods.

The 1D quantum confinement effect in ultrafine ZnO nanorods was investigated using PL spectroscopy. Figure 3 shows room-temperature PL spectra of both ultrafine and thick ZnO nanorods with different mean diameters of 8 ± 3 nm, 9 ± 3 nm, 12 ± 3 nm, and 35 ± 4 nm. The dominant PL peak for the 35-nm-thick ZnO nanorods was observed at 3.285 eV, almost the same PL peak position as for bulk ZnO [22,23]. For ultrafine ZnO

nanorods with diameters of 12, 9, and 8 nm, however, the dominant PL peak was observed at 3.301, 3.316, and 3.327 eV with corresponding PL peak shifts of 16, 31, and 42 meV, respectively. This systematic blue-shift in the PL peak position with decreasing nanorod diameter presumably results from the 1D quantum-confinement effect in ZnO nanorods. The blueshifts observed in this research are also noted to be comparable to those from 6-nm-thick ZnO nanobelts [17]. To clarify this quantum size effect, we calculated the energy shift (ΔE) for a cylindrical potential based on an effective mass model with a simple finite potential barrier. In these calculations, the effective masses of the electrons and the holes of ZnO were $0.28 m_0$, and $1.8 m_0$, respectively [24]. The calculated values of ΔE were 24, 44, and 55 meV for the diameters of 12, 9, and 8 nm, respectively; 8 – 13 meV higher than the experimental data. The larger values in the calculation are presumably due to the Coulomb interaction between electrons and holes being neglected in the calculations, which reduces ΔE . Nevertheless, these simple calculations strongly support the blue-shift in the PL spectra of ultrafine ZnO nanorods being the result of a diameter-dependent quantum-confinement effect.

IV. CONCLUSIONS

ZnO nanorods with extremely narrow diameters of less than 10 nm and a narrow size distribution below 4 nm with a very high aspect ratio of above 300 were prepared on Si substrates at temperatures above 800 °C by using catalyst-free MOCVD. Electron microscopy and SR-XRD studies showed that the ultrafine ZnO nanorods were almost defect-free and of high crystallinity. Furthermore, the excitonic emission peaks in the PL spectra of the ultrafine ZnO nanorods were blue-shifted, presumably because of the quantum confinement effect along the radial direction in ZnO nanorods. Our controlled growth of these quasi-1D quantum building blocks opens significant opportunities for fabrication of oxide-based quantum-device structures for nanometer-scale electronics and photonics and for biological and chemical molecule nanosensor applications.

ACKNOWLEDGMENTS

This work was supported by the Korea Research Foundation Grant (KRF-2002-041-C00098).

REFERENCES

- [1] C. T. White and T. N. Todorov, *Nature* **411**, 649 (2001).
- [2] A. Javey, J. Guo, Q. Wang, M. Lundstrom and H. Dai, *Nature* **424**, 654 (2003).

- [3] Y. Cui, Q. Wei, H. Park and C. M. Lieber, *Science* **293**, 1289 (2001).
- [4] Ph. Avouris, *Acc. Chem. Res.* **35**, 1026 (2002).
- [5] S. J. Tans, R. M. Verschueren and C. Dekker, *Nature* **393**, 49 (1998).
- [6] Y. Huang, X. Duan, Y. Cui, L. Lauhon, K. Kim and C. M. Lieber, *Science* **294**, 1313 (2001).
- [7] X. Duan, Y. Huang, Y. Cui, J. Wang and C. M. Lieber, *Nature* **409**, 66 (2001).
- [8] T. W. Kang and H. M. Kim, *Met. Mater. Int.* **10**, 367 (2004).
- [9] H-M. Kim, H. Lee, S. I. Kim, S. R. Ryu, T. W. Kang, D. Y. Kim, K. S. Chung, J. P. Hong and Y. D. Woo, *J. Korean Phys. Soc.* **45**, 701 (2004).
- [10] M. Huang, S. Mao, H. Feick, H. Yan, Y. Wu, H. Kind, E. Weber, R. Russo and P. Yang, *Science* **292**, 1897 (2001).
- [11] M. S. Gudiksen, J. Wang and C. M. Lieber, *J. Phys. Chem. B* **106**, 4036 (2002).
- [12] S. Hong, T. Joo, W. I. Park, Y. H. Jun and G-C. Yi, *Appl. Phys. Lett.* **83**, 4157 (2003).
- [13] R. T. Senger and K. K. Bajaj, *Phys. Rev. B* **68**, 045313 (2003).
- [14] S-W. Kim, M. Ueda, S. Fujita and S. Fujita, *J. Korean Phys. Soc.* **45**, 803 (2004).
- [15] H. J. Chang, C. Z. Lu, Y. Wang, C-S. Son, S-I. Kim, Y-H. Kim, and I-H. Choi, *J. Korean Phys. Soc.* **45**, 956 (2004).
- [16] Y. Gu, I. L. Kuskovsky, M. Yin, S. O'Brien and G. F. Neumark, *Appl. Phys. Lett.* **85**, 3833 (2004).
- [17] X. Wang, Y. Ding, C. J. Summers and Z. L. Wang, *J. Phys. Chem. B* **108**, 8773 (2004).
- [18] W. I. Park, D. H. Kim, S-W. Jung and G-C. Yi, *Appl. Phys. Lett.* **80**, 4232 (2002); W. I. Park, G-C. Yi, M. Kim and S. J. Pennycook, *Adv. Mater.* **14**, 841 (2003).
- [19] W. J. Li, E. W. Shi, W. Z. Zhong and Z. W. Yin, *J. Cryst. Growth* **203**, 186 (1999).
- [20] Z. L. Wang, X. Y. Kong and J. M. Zuo, *Phys. Rev. Lett.* **91**, 185502 (2003).
- [21] Y. A. Jeon, K. S. No, J. S. Kim and Y. S. Yoon, *Met. Mater. Int.* **9**, 383 (2003).
- [22] S. W. Jung, W. I. Park, H. D. Cheong, G-C. Yi, H. M. Jang, S. Hong and T. Joo, *Appl. Phys. Lett.* **80**, 1924 (2002).
- [23] J. Y. Park, Y. S. No, B. J. Park, H. W. Lee, J. W. Choi, J. S. Kim, Y. Ermakov, S. J. Yoon, Y. J. Oh and W. K. Choi, *Met. Mater. Int.* **10**, 351 (2004).
- [24] L. E. Brus, *J. Chem. Phys.* **80**, 4403 (1984).